Anticonvection with an inclined temperature gradient

I. B. Simanovskii,[1] P. Colinet,[2] A. A. Nepomnyashchy,[1] and J.-C. Legros[2]
[1]*Department of Mathematics, Technion–Israel Institute of Technology, 32000 Haifa, Israel*
[2]*Service de Chimie Physique EP, Université Libre de Bruxelles, Case Postale 165-62, 50 Avenue F. D. Roosevelt, 1050 Bruxelles, Belgium*

(Received 17 December 2001; revised manuscript received 10 June 2002; published 19 November 2002)

Anticonvection, caused by external heating from above in the presence of heat sources (or sinks) homogeneously distributed on the interface, is investigated in the presence of an imposed horizontal temperature gradient. Numerical finite-difference simulations of the finite-amplitude convective regimes have been performed for the two-layer system of fluids. The interface is assumed to be flat. We discuss different scenarios of transition between multicell regimes characteristic of a vertical temperature gradient, and unicell structures induced by horizontal gradients. The coexistence of these two regimes in sufficiently long cavities has been obtained. Regular oscillations are also predicted in other situations.

DOI: 10.1103/PhysRevE.66.056305 PACS number(s): 44.25.+f

I. INTRODUCTION

It is well known [1] that in a horizontal fluid layer heated from above, all the disturbances decay either in a monotonic or oscillatory manner, and the mechanical equilibrium state is realized in the system. Paradoxically, it is not actually correct in the presence of the interface between two fluids. It was shown by Welander [2] that when the temperature gradient is directed vertically upwards, the two-layer system, consisting of two immiscible viscous fluids of infinite thicknesses, may become unstable with respect to monotonic disturbances. The specific non-Rayleigh mechanism of instability (anticonvection) is realized in the system. This mechanism of instability may appear only under the definite condition that fluids with considerably different physical properties must be taken. Particularly, the heat expansion coefficient of the upper layer must be much smaller than that of the lower layer, and the thermal diffusivity of the lower layer must be much higher than that of the upper one (or vice versa). The linear stability boundaries (for layers of finite thicknesses) were determined in Ref. [3] and the finite-amplitude regimes of anticonvection were obtained in Ref. [4] (see also Refs. [5,6]).

The phenomenon of anticonvection was considered as rather exotic during a long time. As the matter of fact, only one physical system (water-mercury) satisfying the conditions for the existence of anticonvection was found [3]. It turns out however that the appearance of anticonvection can be simplified when the interface serves as a source or sink of heat [7]. Moreover, it was found in Refs. [8,9] that in the presence of an interfacial heat source (sink) the anticonvection could be generated in *any* system of two semi-infinite layers. It was shown that the anticonvection appears in the situation where the temperature gradient in one fluid is much smaller than that in another fluid. The difference between the temperature gradients, sufficient for the appearance of the anticonvection, can be caused by the natural difference of thermophysical parameters of fluids, as in the case of the water-mercury system, or it can be produced artificially by heating or cooling the interface.

The general analysis of conditions for the appearance of anticonvection in the system of layers with finite thicknesses was done in Ref. [10]. The nonlinear regimes of anticonvection in a system of layers with finite thicknesses in the presence of heat release on the interface were investigated in Ref. [11].

Under experimental conditions, the temperature gradient in the system is not perfectly vertical. The horizontal component of the temperature gradient generates a convective flow. The influence of this flow on the convective patterns generated by the vertical temperature gradient has been investigated in detail in the case of the usual Rayleigh-Benard convection (see Refs. [13–15]). The stability of thermocapillary flows with the inclined temperature gradient was studied in Refs. [16,17]. To our knowledge, the interaction between the anticonvection caused by heating from above and the convective flow produced by the horizontal component of the temperature gradient has never been studied before. That is the goal of the present paper.

In Sec. II, the mathematical formulation of the problem and the numerical method are presented. Section III is devoted to the consideration of flows generated by the joint action of the vertical and horizontal components of the temperature gradient and heat release on the interface. Section IV contains some concluding remarks.

II. FORMULATION OF THE PROBLEM AND THE NUMERICAL METHOD

Let a rectangular cavity with solid boundaries be filled by two immiscible viscous fluids (see Fig. 1). The temperature on the horizontal plates $z=a_1$ and $z=-a_2$ is fixed in the following way: $T(x,y,a_1,t)=-A_h x+\theta, T(x,y,-a_2,t)=-A_h x, A_h>0$. The vertical lateral boundaries $x=0$ and $x=l$ are heat insulated. The constant heat release at the rate Q_0 (Q_0 may be positive or negative) is set on the interface. The interface is assumed to be flat and undeformable. We assume also that the thicknesses of the layers are sufficiently large, so that the thermocapillary effect is negligible as compared to the buoyancy effect. A more detailed discussion of these assumptions is given in the Appendix. All variables referring to the upper layer are marked by index 1, and the variables referring to the lower layer are marked by index 2.

Let us use the following notations:

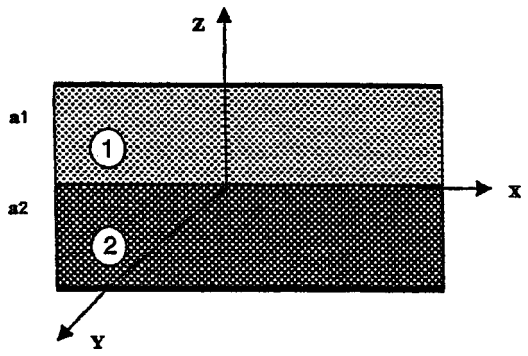

FIG. 1. Geometrical configuration of the two-layer system and coordinate axes.

$$\rho=\rho_1/\rho_2, \quad \nu=\nu_1/\nu_2, \quad \eta=\eta_1/\eta_2, \quad \kappa=\kappa_1/\kappa_2,$$

$$\chi=\chi_1/\chi_2, \quad \beta=\beta_1/\beta_2, \quad a=a_2/a_1, \quad L=l/a_1.$$

Here ρ_m, ν_m, η_m, κ_m, χ_m, β_m, and a_m are, respectively, the densities, kinematic and dynamic viscosities, heat conductivity, thermal diffusivity, heat expansion coefficient, and the thickness of the mth layer ($m=1,2$). As the units of length, time, velocity, pressure, and temperature, we choose a_1, a_1^2/ν_1, ν_1/a_1, $\rho_1\nu_1^2/a_1^2$, and θ, respectively. The problem is considered in the framework of the Boussinesq approximation [1] (for details, see the Appendix). The nonlinear equations governing convection in a two-layer system have the following form [12]:

$$\frac{\partial\vec{v}_m}{\partial t}+(\vec{v}_m\cdot\vec{\nabla})\vec{v}_m=-\vec{\nabla}p_m+c_m\nabla^2\vec{v}_m+b_m\mathrm{Gr}T_m\vec{\gamma},$$

$$\frac{\partial T_m}{\partial t}+\vec{v}_m\cdot\vec{\nabla}T_m=\frac{d_m}{\mathrm{Pr}}\nabla^2T_m, \tag{1}$$

$$\vec{\nabla}\cdot\vec{v}_m=0.$$

Here, $\vec{v}_m=(v_{mx},v_{my},v_{mz})$ is the velocity vector, T_m is the temperature, and p_m is the pressure in the mth fluid; $c_1=b_1=d_1=1$; $c_2=1/\nu$, $b_2=1/\beta$, $d_2=1/\chi$; $\mathrm{Gr}=g\beta_1\theta a_1^3/\nu_1^2$ is the Grashof number, $\mathrm{Pr}=\nu_1/\chi_1$ is the Prandtl number for the liquid in layer 1, $\vec{\gamma}$ is the unit vector directed vertically upward. The conditions on the isothermic rigid horizontal boundaries are

$$v_1=0, \quad T_1=-\epsilon x+1, \quad z=1,$$

$$v_2=0, \quad T_2=-\epsilon x, \quad z=-a, \tag{2}$$

where $\epsilon=A_h a_1/\theta>0$ is the nondimensional parameter characterizing the horizontal component of the temperature gradient. The boundary conditions on the interface $z=0$ include conditions for the tangential stresses,

$$\eta\frac{\partial v_{1x}}{\partial z}=\frac{\partial v_{2x}}{\partial z}, \quad \eta\frac{\partial v_{1y}}{\partial z}=\frac{\partial v_{2y}}{\partial z}, \quad z=0; \tag{3}$$

the continuity of the velocity field,

$$v_1=v_2, \quad z=0; \tag{4}$$

the continuity of the temperature field,

$$T_1=T_2, \quad z=0; \tag{5}$$

and the continuity of the heat flux normal components,

$$\kappa\frac{\partial T_1}{\partial z}=\frac{\partial T_2}{\partial z}-\kappa\frac{\mathrm{Gr}_Q}{\mathrm{Gr}}, \quad z=0, \tag{6}$$

where $\mathrm{Gr}_Q=g\beta_1Q_0a_1^4/\nu_1^2\kappa_1$ is the modified Grashof number determined by the intensity of the interfacial heat release. The conditions on the solid lateral boundaries, which are assumed to be thermally insulated, are

$$v_m=0, \quad \frac{\partial T_m}{\partial x}=0, \quad m=1,2, \quad x=0,L. \tag{7}$$

For two-dimensional flows ($v_{my}=0$; the fields of physical variables do not depend on y), we can introduce the stream function ψ,

$$v_{mx}=\frac{\partial\psi_m}{\partial z}, \quad v_{mz}=-\frac{\partial\psi_m}{\partial x} \quad (m=1,2).$$

Eliminating the pressure and defining the vorticity

$$\phi_m=\frac{\partial v_{mz}}{\partial x}-\frac{\partial v_{mx}}{\partial z},$$

we can rewrite the boundary-value problem in the following form:

$$\frac{\partial\phi_m}{\partial t}+\frac{\partial\psi_m}{\partial z}\frac{\partial\phi_m}{\partial x}-\frac{\partial\psi_m}{\partial x}\frac{\partial\phi_m}{\partial z}=c_m\nabla^2\phi_m+b_m\mathrm{Gr}\frac{\partial T_m}{\partial x}, \tag{8}$$

$$\nabla^2\psi_m=-\phi_m, \tag{9}$$

$$\frac{\partial T_m}{\partial t}+\frac{\partial\psi_m}{\partial z}\frac{\partial T_m}{\partial x}-\frac{\partial\psi_m}{\partial x}\frac{\partial T_m}{\partial z}=\frac{d_m}{\mathrm{Pr}}\nabla^2T_m \quad (m=1,2), \tag{10}$$

$$\psi_1=\frac{\partial\psi_1}{\partial z}=0, \quad T_1=-\epsilon x+1, \quad z=1, \tag{11}$$

$$\psi_2=\frac{\partial\psi_2}{\partial z}=0, \quad T_2=-\epsilon x, \quad z=-a, \tag{12}$$

$$\psi_1=\psi_2=0, \quad \frac{\partial\psi_1}{\partial z}=\frac{\partial\psi_2}{\partial z}, \quad \eta\phi_1=\phi_2, \quad z=0, \tag{13}$$

$$T_1=T_2, \quad \kappa\frac{\partial T_1}{\partial z}=\frac{\partial T_2}{\partial z}-\kappa\frac{\mathrm{Gr}_Q}{\mathrm{Gr}}, \tag{14}$$

$$\psi_m = \frac{\partial \psi_m}{\partial x} = \frac{\partial T_m}{\partial x} = 0, \tag{15}$$

$$m = 1,2, \quad x = 0, L.$$

In the absence of the horizontal temperature gradient ($\epsilon = 0$), the system (8)–(15) has a solution

$$\psi_1 = \psi_2 = 0, \quad T_1^{(0)} = 1 + A_1(z-1), \quad T_2^{(0)} = A_2(z+a), \tag{16}$$

$$A_1 = \frac{1 - a\kappa\,\mathrm{Gr}_Q/\mathrm{Gr}}{1 + a\kappa}, \quad A_2 = \frac{\kappa(1 + \mathrm{Gr}_Q/\mathrm{Gr})}{1 + a\kappa}, \tag{17}$$

which corresponds to the mechanical equilibrium state. It is known, however, that the mechanical equilibrium state is unstable with respect to the anticonvective instability mechanism in a certain region of parameters Gr and Gr_Q [10]. If $\epsilon \neq 0$, an analytical solution can be obtained only in the limit $L \to \infty$. This solution describes a parallel flow, $\psi_m = \psi_m(z)$, and the distortion of the temperature profile (16) due to the advection of heat by this flow, $\theta_m(z)$ ($m = 1,2$). The explicit expressions for functions $\psi_m(z)$ and $\theta_m(z)$ are given in the Appendix.

In the finite cavity ($L < \infty$) the flow is nearly parallel in the middle part of the cavity (core region), while in the end regions near the lateral walls the flow is essentially nonparallel. In order to investigate the development of the anticonvection on the background of the convective flow, generated by the horizontal temperature gradient, we have performed nonlinear simulations of the boundary-value problem (8)–(15). The finite-difference method has been used. Equations and boundary conditions were approximated on a uniform mesh using a second-order approximation for the spatial coordinates. The nonlinear equations were solved using an explicit scheme on a rectangular uniform mesh 56×56 ($L = 4$), 84×56 ($L = 16$), 168×56 ($L = 32$). The Poisson equation was solved by the iterative Liebman successive overrelaxation method on each time step: the accuracy of the solution was 10^{-4}. The Kuskova and Chudov formulas [18], providing second-order accuracy, were used for the approximation of the vorticity on the solid boundaries. At the interface the expression for the vorticity is approximated with second-order accuracy for the spatial coordinates and have a form

$$\phi_1 = \frac{-2[\psi_2(x,-\Delta z) + \psi_1(x,\Delta z)]}{(\Delta z)^2(1+\eta)}, \tag{18}$$

$$\phi_2(x,0) = \eta\phi_1(x,0). \tag{19}$$

Here Δx, Δz are the mesh sizes for the corresponding coordinates. The temperatures on the interfaces were calculated by the second-order approximation formulas

$$T_1(x,0) = T_2(x,0) = \frac{[4T_2(x,-\Delta z) - T_2(x,-2\Delta z)] + \kappa[4T_1(x,\Delta z) - T_1(x,2\Delta z)]}{3(1+\kappa)}. \tag{20}$$

The details of the numerical method can be found in the book of Simanovskii and Nepomnyashchy [12].

III. NUMERICAL RESULTS

In this section we present the results of the numerical solution of the boundary-value problem (8)–(15) for the real two-liquid system silicone oil (10 cS)–ethylene glycol (1 S $= 1\ \mathrm{cm}^2/\mathrm{s}$) with the following set of parameters: $\rho = 0.846$, $\eta = 0.549$, $\nu = 0.6493$, $\kappa = 0.6194$, $\chi = 1.096$, $\beta = 1.4516$, the Prandtl number $\mathrm{Pr} = 94$. The calculations were performed with $a = 1$.

In the case $\epsilon = 0$, the mechanical equilibrium state (16), (17) becomes unstable due to the anticonvective instability if Gr is large enough. As was explained in Ref. [10], one can expect the appearance of anticonvection in two cases: (1) $0 < A_1 \ll A_2$, (2) $0 < A_2 \ll A_1$. According to formulas (17), the first case takes place as $\mathrm{Gr}_Q \geqslant 0$ and Gr is close but larger than $a\kappa\mathrm{Gr}_Q$. Similarly, the second case takes place as $\mathrm{Gr}_Q < 0$, and Gr is close but larger than $|\mathrm{Gr}_Q|$ [see Fig. 2(a)]. Note that in the case $0 < \mathrm{Gr} < a\kappa\mathrm{Gr}_Q$ one obtains that $A_1 < 0$, $A_2 > 0$, which corresponds to the profile of Fig. 2(b). Similarly, in the case $\mathrm{Gr}_Q < 0$, $0 < \mathrm{Gr} < |\mathrm{Gr}_Q|$ the temperature profile is shown in Fig. 2(c). Typical stationary anticonvective flows in the former case ($0 < A_1 \ll A_2$) are shown in Fig. 3. There are two different streamline patterns: pattern *A* [Fig. 3(a)] and pattern *B* [Fig. 3(b)]. In the case of the pattern *A*, there exists a negative temperature deviation $T_m(x,z) - T_m^0(z)$ in the middle of the cavity [Fig. 3(c)], which produces an extensive descending motion in the upper layer (with nearly vanishing temperature gradient), and a relatively weak viscosity-induced ascending motion in the lower layer (with a strong positive gradient) near the interface [Fig. 3(a)]. Near the lateral boundaries, a positive deviation of the temperature generates an ascending motion in the upper layer and a descending motion near the interface in the lower

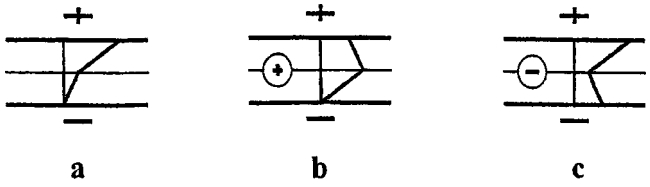

FIG. 2. Temperature profiles in the two-layer system under the joint action of the external heating and heat source (sink) on the interface. The anticonvection appears in the case (a).

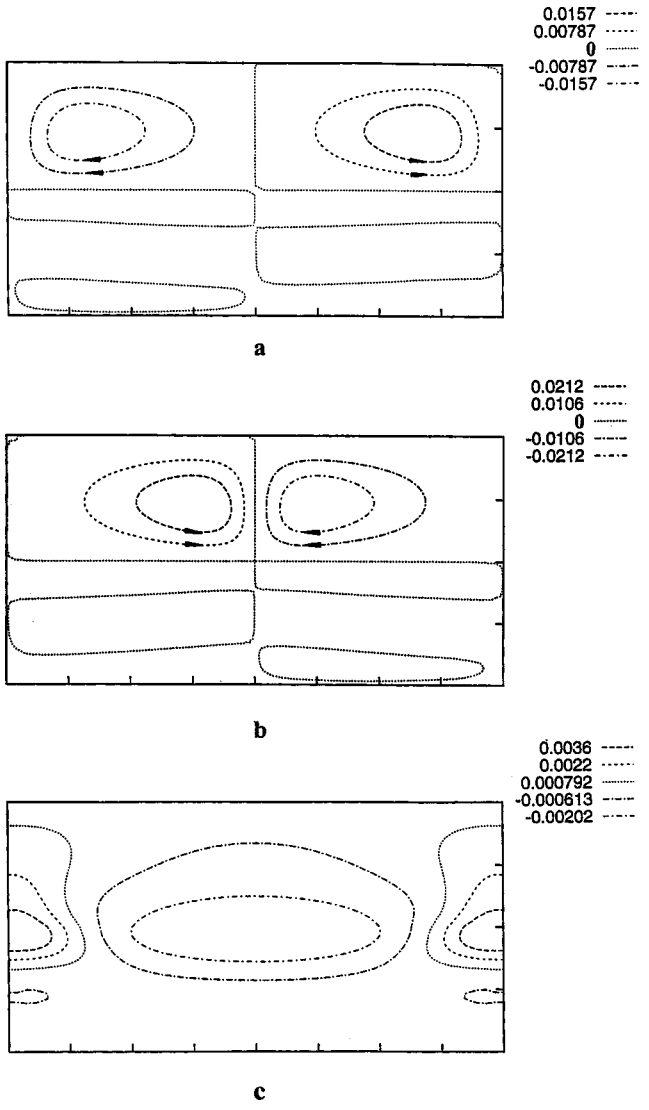

FIG. 3. Streamlines (a),(b) and isolines of the temperature deviations (c) for the steady anticonvective motions (Gr=3717, Gr_Q =6000, $L=4$, $\epsilon=0$).

layer, in a similar way. In the case of pattern *B*, the negative temperature disturbance is located near the lateral boundaries, and the positive temperature disturbance is located in the middle of the cavity. For both kinds of patterns,

$$\psi_m(x,z,t) = -\psi_m(L-x,z,t), \tag{21}$$

$$T_m(x,z,t) = T_m(L-x,z,t). \tag{22}$$

Let us consider now the influence of a horizontal temperature gradient on the structure described above. For any ϵ, the symmetry conditions (21), (22) are violated. In the case of pattern *A*, the positive vortex near the cold wall in the upper layer is suppressed [see Figs. 4(a) and 4(b)]. Finally, the unicell structure, typical for heating from the lateral wall, is established in the upper layer [Fig. 4(c)]; the fields of temperature deviations $T'_m(x,z)=T_m(x,z)-T^0_m(z)-\epsilon x$ are shown in Fig. 4(d). Similarly, in the case of pattern *B* the positive vortex is suppressed near the hot wall.

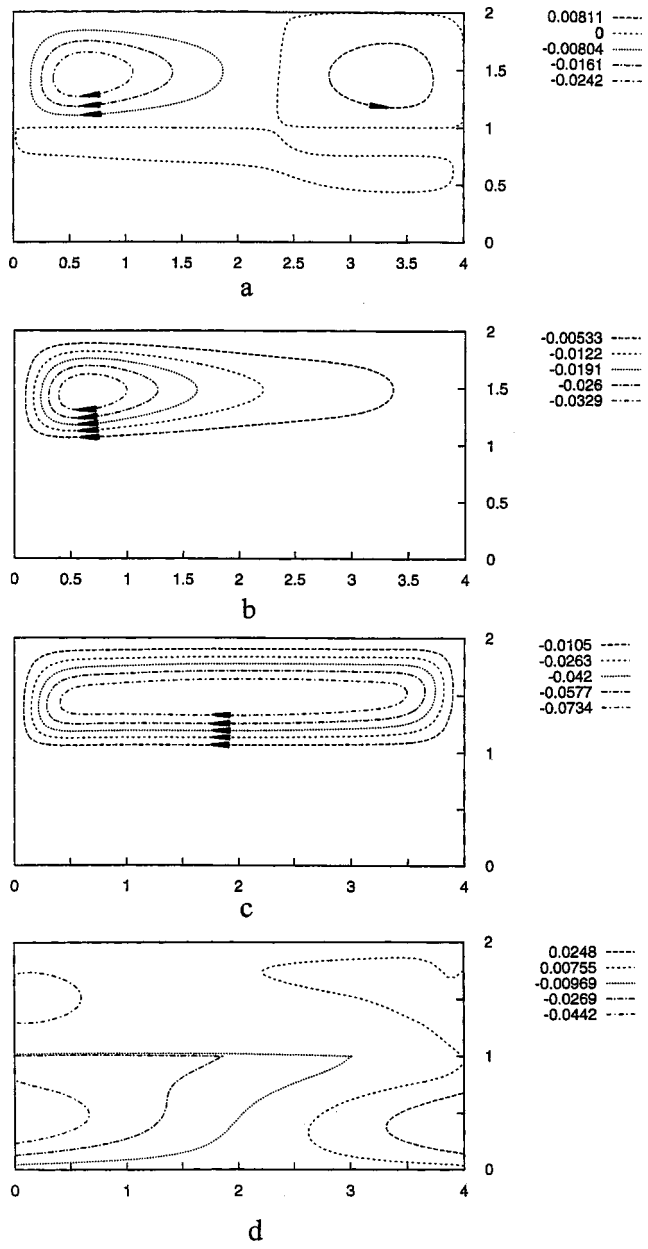

FIG. 4. Streamlines (a)–(c) and isolines of the temperature deviations (d) for Gr=3717, $\mathrm{Gr}_Q=6000$, $L=4$; (a) $\epsilon=1.45\times10^{-3}$, (b) $\epsilon=3\times10^{-3}$; (c),(d) $\epsilon=5\times10^{-2}$.

With the decrease in the Grashof number ($\mathrm{Gr}_Q>0$, $0<\mathrm{Gr}<a\kappa\mathrm{Gr}_Q$ or $\mathrm{Gr}_Q<0$, $0<\mathrm{Gr}<|\mathrm{Gr}_Q|$), the signs of the equilibrium temperature gradients A_1 and A_2 become different [Figs. 2(b) and 2(c)]. In the case $\epsilon=0$, the anticonvection and the Rayleigh-Benard instability mechanism act simultaneously (see pattern *B* in Fig. 5). The influence of the Rayleigh-Benard (bulk) instability mechanism leads to an obvious change of the roll's shape in comparison with that of the pure anticonvection, which is essentially connected with the interface [cf. Fig. 3(b)]. The suppression of the positive vortex which is located near the hot wall is shown in Figs. 6(a)–6(c). Temperature deviations corresponding to the last structure are presented in Fig. 6(d). The results of simulations described above are summarized in Fig. 7. Note that in

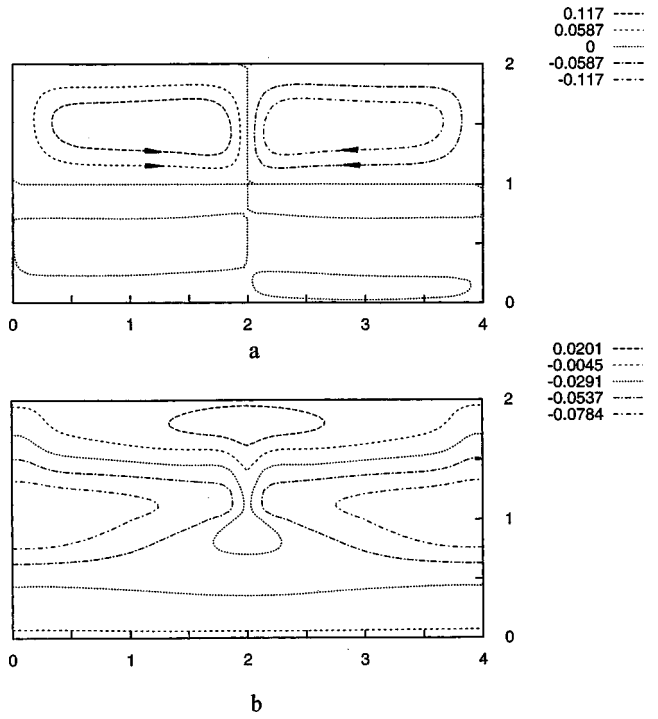

FIG. 5. Streamlines (a) and isolines of the temperature deviations (b) in the region of the combined action of anticonvection and Rayleigh-Benard convection for $\mathrm{Gr}=3000$, $\mathrm{Gr}_Q=6000$, $L=4$, $\epsilon=0$.

the case of the pure anticonvection the transition to the unicellular flow takes place for much smaller values of ϵ. A similar evolution of the flow pattern has been observed in the case $\mathrm{Gr}_Q<0$, $\mathrm{Gr}>\mathrm{Gr}_Q$ (see Fig. 8).

Another scenario of the transition to the unicell structure takes place in the case when the anticonvection and the Rayleigh-Benard instability mechanism act simultaneously ($\mathrm{Gr}_Q<0$, $\mathrm{Gr}<|\mathrm{Gr}_Q|$, $A_1>0$, $A_2<0$). In the absence of the horizontal temperature gradient ($\epsilon=0$) streamlines and temperature deviations satisfy the symmetry conditions (21), (22) [see Figs. 10(a) and 10(b)]. With the increase of ϵ the symmetry conditions are violated and the negative vortex suppresses the positive one in the lower layer [see Figs. 9(c) and 9(d)].

At the definite region $0.007<\epsilon<0.0095$ the steady motion becomes unstable and regular oscillations develop in the system. The sizes of the vortices are not changed, but the shape of the streamlines and the intensity of the motion changes slightly [see Figs. 9(e) and 9(f)]. The period of oscillations is almost independent of ϵ.

As $\epsilon>0.0095$ the steady one-vortex motion, filling in practice the whole volume in the bottom layer, is realized in the system [Figs. 9(g) and 9(h)]. When ϵ grows, the maximum of the stream function for the one-vortex motion is shifted towards the hot lateral wall. The transitions between different flow regimes are shown in Fig. 10.

Now let us consider the case of long cavities ($L=16$). The streamline pattern corresponding to the pure anticonvective flow for $\mathrm{Gr}_Q>0$, $\mathrm{Gr}>a\kappa\mathrm{Gr}_Q$ ($0<A_1\ll A_2$), $\epsilon=0$ is shown in Fig. 11(a). Since the temperature gradients A_1 and

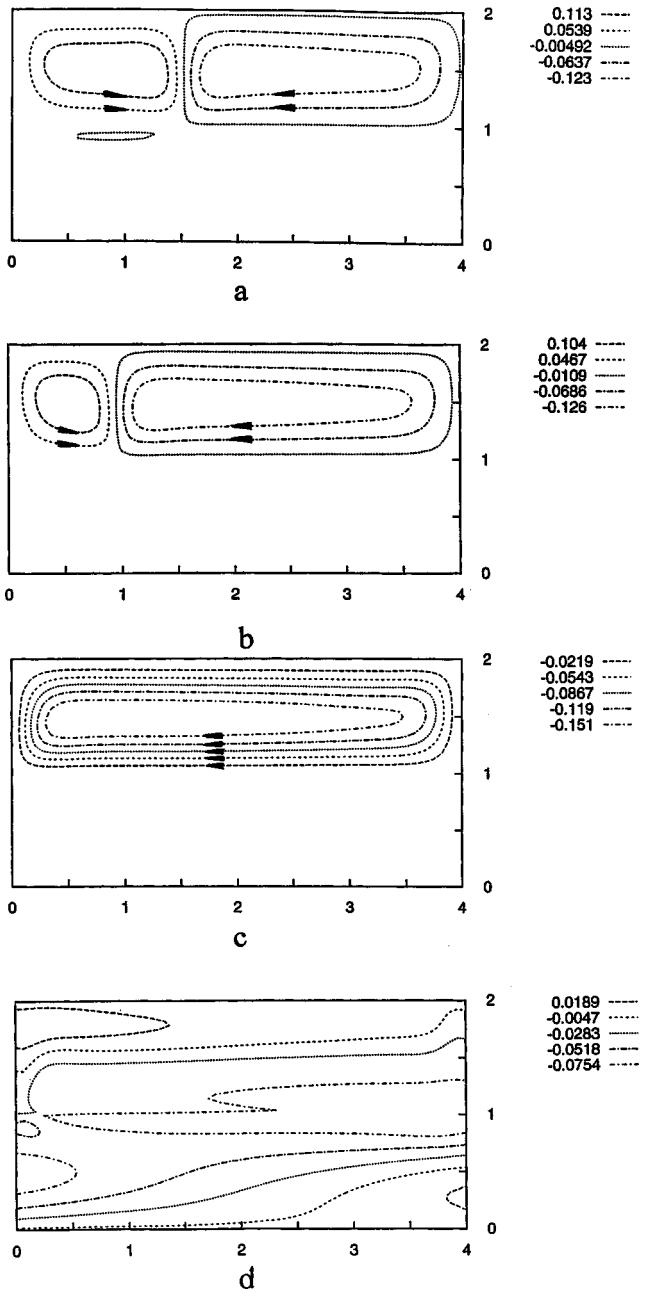

FIG. 6. Streamlines (a)–(c) and isolines of the temperature deviations (d) for $\mathrm{Gr}=3000$, $\mathrm{Gr}_Q=6000$, $L=4$; (a) $\epsilon=1.1\times10^{-2}$; (b) $\epsilon=1.5\times10^{-2}$; (c),(d) $\epsilon=5\times10^{-2}$.

A_2 are positive, anticonvection is the only possible mechanism of instability in the system. The streamlines and the temperature fields satisfy the symmetry conditions (21), (22). One can see the rather intensive motion in the upper layer with the nearly vanishing temperature gradient and the multistore structure in the lower layer, characterized by the strong temperature gradient.

The inclined horizontal temperature gradient leads to the violation of symmetry conditions (21), (22) in the case $\epsilon>0$. The most intensive vortices are situated in the top layer near the cold wall [see Figs. 11(b)–11(e)]. With the increase of A_h the intensity of the motion grows and the vortices have the tendency to become longer.

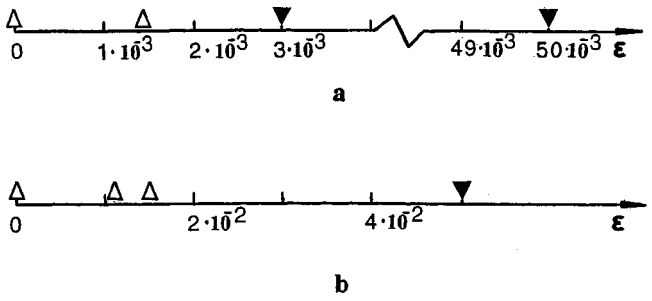

FIG. 7. Diagrams of regimes (a) in the case of pure anticonvection, Gr=3717, $Gr_Q=6000$, $L=4$; (b) in the case of the combined action of anticonvection and Rayleigh-Benard convection, Gr =3000, $Gr_Q=6000$, $L=4$. △, two-vortex motion; ▼, one-vortex motion.

In the case $Gr_Q<0$, $Gr>|Gr_Q|$ ($0<A_2\ll A_1$, $\epsilon=0$) the most intensive motion takes place in the lower layer and the multistore structure is realized in the upper layer [see Fig. 12(a)]. The inclusion of the horizontal temperature gradient leads to the suppression of the vortices near the cold wall. At the larger values of ϵ, the intensity of these vortices decreases [Figs. 12(b) and 12(c)]. Finally, the long cells become preferable in the system [Fig. 12(d)].

Let us take the case $L=32$, $Gr_Q<0$. If $\epsilon=0$, since A_1 and A_2 are positive, anticonvection is realized in the system. The symmetric motion, presented in Fig. 13(a), corresponds to the nearly vanishing temperature gradient in the lower layer and the strong positive gradient in the upper layer. With the increase of ϵ the symmetry of the structure is destroyed and the most intensive motion takes place mainly near the hot wall [Figs. 13(b) and 13(c)]. At larger values of ϵ one can obtain the coexistence of the ''multicell'' structure near the hot wall and the one-vortex motion near the cold wall [see Fig. 13(d)].

IV. CONCLUSION

The interaction between the anticonvection generated by the external heating from above and the interfacial heat release, and the flow, caused by the inclined horizontal temperature gradient, is investigated. Nonlinear finite-amplitude convective regimes in the real two-liquid system silicone oil (10 cS)–ethylene glycol have been studied. Different sce-

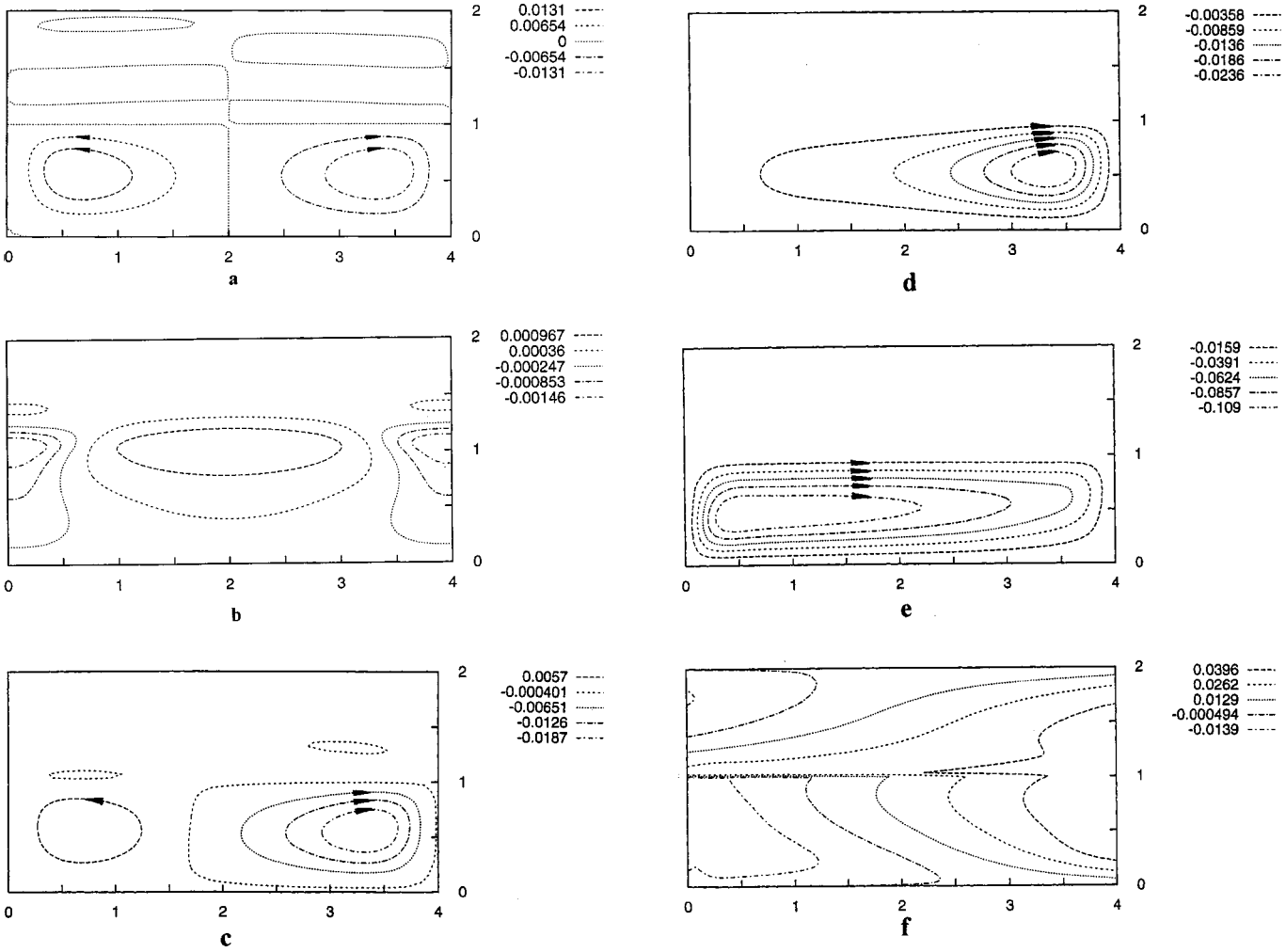

FIG. 8. Streamlines (a),(c)–(e) and isolines of the temperature deviations (b),(f) for Gr=15 000, $Gr_Q=-15\,000$, $L=4$; (a),(b) $\epsilon=0$; (c) $\epsilon=2.78\times10^{-4}$; (d) $\epsilon=5\times10^{-4}$; (e),(f) $\epsilon=5\times10^{-3}$.

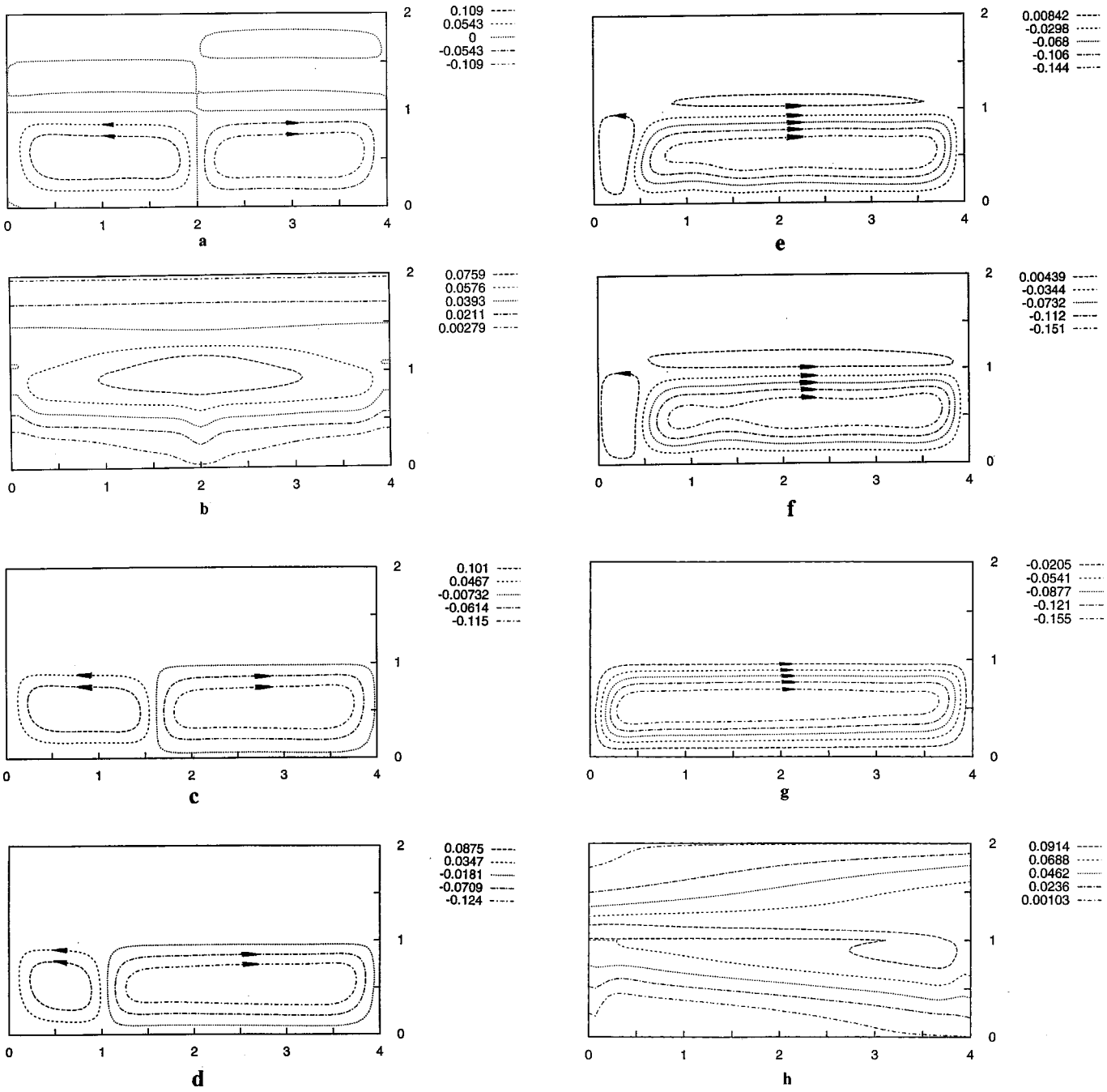

FIG. 9. Streamlines (a),(c)–(g) and isolines of temperature deviations (b),(h) for $\mathrm{Gr}=11\,500$, $\mathrm{Gr}_Q=-15\,000$, $L=4$; (a),(b) $\epsilon=0$; (c) $\epsilon=2.5\times10^{-3}$; (d) $\epsilon=5\times10^{-3}$; (e),(f) $\epsilon=8.7\times10^{-3}$; (g),(h) $\epsilon=5\times10^{-2}$.

narios of transition to the unicell structures are considered.

It is remarkable that we observe typically *stationary* multicellular patterns, though the instability of the *flow* (A7), (A8) with respect to two-dimensional disturbances should be obviously *oscillatory*. This phenomenon was formerly observed in the case of a buoyant-thermocapillary flow generated by a horizontal temperature gradient (see Ref. [19] and references therein). Recently, this phenomenon was explained by the analysis of the influence of lateral boundaries [20].

Nevertheless, in the definite region of parameter ϵ, characterizing the horizontal component of the temperature gradient, regular oscillations develop in the system. The coexistence of the multicell structure near the hot wall and the one-vortex motion near the cold wall in the long cavities have been observed.

ACKNOWLEDGMENTS

This work was supported by the Israeli Science Foundation. The authors acknowledge financial support by the European Union, through the ICOPAC Research Training Network HPRN-CT-2000-00136. P.C. acknowledges financial support from the Fonds National de la Recherche Scientifique (Belgium).

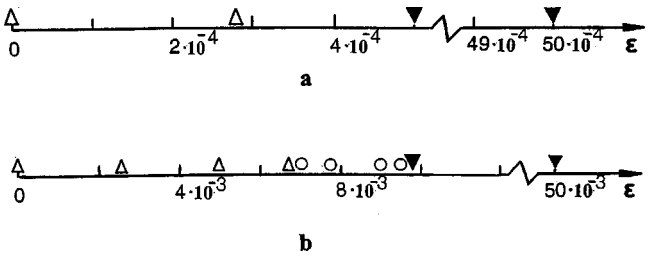

FIG. 10. Diagrams of regimes (a) in the case of pure anticonvection, $\mathrm{Gr}=15\,000$, $\mathrm{Gr}_Q=-15\,000$, $L=4$; (b) in the case of the combined action of anticonvection and Rayleigh-Benard convection, $\mathrm{Gr}=11\,500$, $\mathrm{Gr}_Q=-15\,000$, $L=4$. △, two-vortex steady motion; ○, two-vortex oscillatory motion; ▼, one-vortex steady motion.

APPENDIX: JUSTIFICATION OF THE MODEL

As was mentioned in Sec. II, the consideration of the anticonvection is given under two assumptions: (1) the deformation of the interface is disregarded, (2) the thermocapillary effect is neglected. Let us discuss the physical origin and the validity conditions of these assumptions.

(1) The deformation of the interface is a non-Boussinesq effect that has to be disregarded when the Boussinesq approximation is used for the description of the buoyancy effect [21,12]. Indeed, the Boussinesq approximation is based on the assumption $\beta_1\theta\ll 1$, while the Grashof number $\mathrm{Gr}=g\beta_1\theta a_1^3/\nu_1^2=O(1)$. Thus, the Galileo number $\mathrm{Ga}=g\beta_1^3/\nu_1^2=\mathrm{Gr}/\beta_1\theta$ is assumed to be infinitely large. The deformation of the interface caused by the natural convective flow is inversely proportional to Ga and thus is negligible in the region of validity of the Boussinesq approximation (except the case of two fluids with very close densities [12]). The consideration of the interfacial deformation without taking into account other non-Boussinesq effects can lead to artifacts (for more details, see Ref. [22]).

(2) In the presence of the thermocapillary effect (the surface tension σ is a function of temperature T), the boundary conditions (3) include additional terms:

$$\eta\frac{\partial v_{1x}}{\partial z}=\frac{\partial v_{2x}}{\partial z}-\frac{d\sigma}{dT}\frac{\partial T}{\partial x},\qquad \eta\frac{\partial v_{1y}}{\partial z}=\frac{\partial v_{2y}}{\partial z}-\frac{d\sigma}{dT}\frac{\partial T}{\partial y},$$

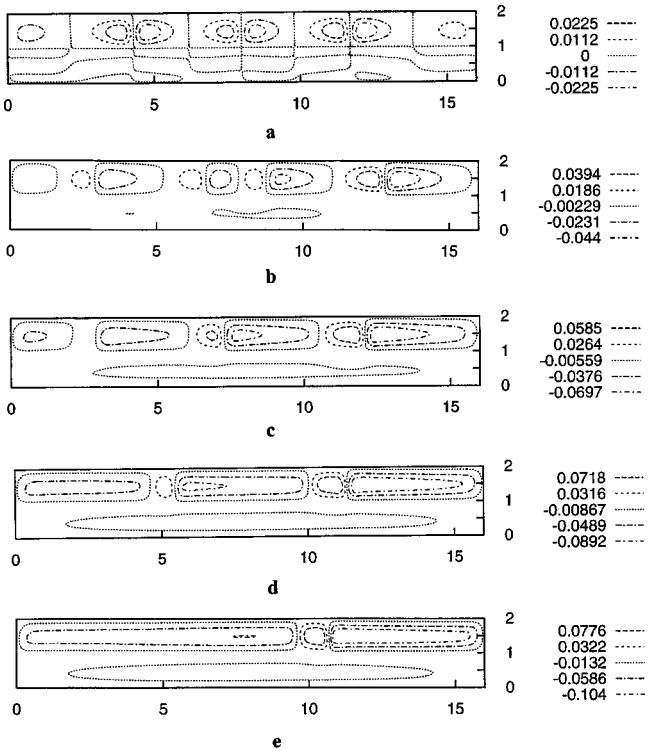

FIG. 11. Streamlines for $\mathrm{Gr}=3717$, $\mathrm{Gr}_Q=6000$, $L=16$: (a) $\epsilon=0$, (b) $\epsilon=0.0145$, (c) $\epsilon=0.05$, (d) $\epsilon=0.1$, (e) $\epsilon=0.15$.

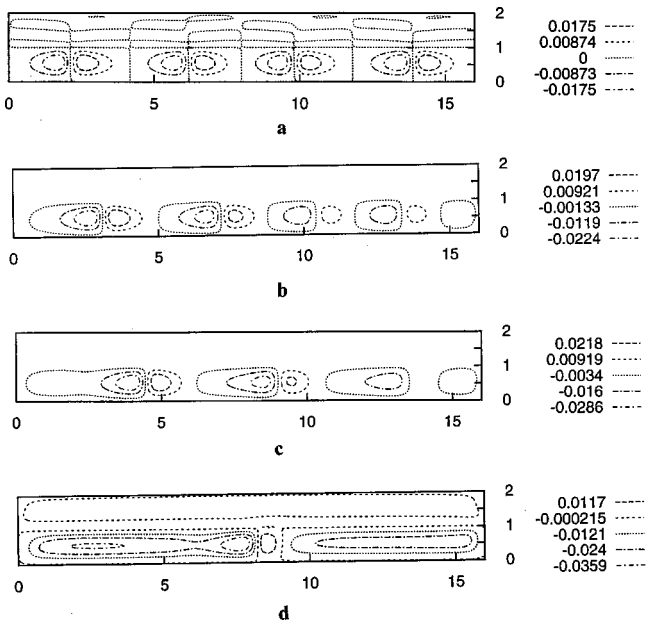

FIG. 12. Streamlines for $\mathrm{Gr}=15\,000$, $\mathrm{Gr}_Q=-15\,000$, $L=16$: (a) $\epsilon=0$, (b) $\epsilon=0.001$, (c) $\epsilon=0.003$, (d) $\epsilon=0.01$.

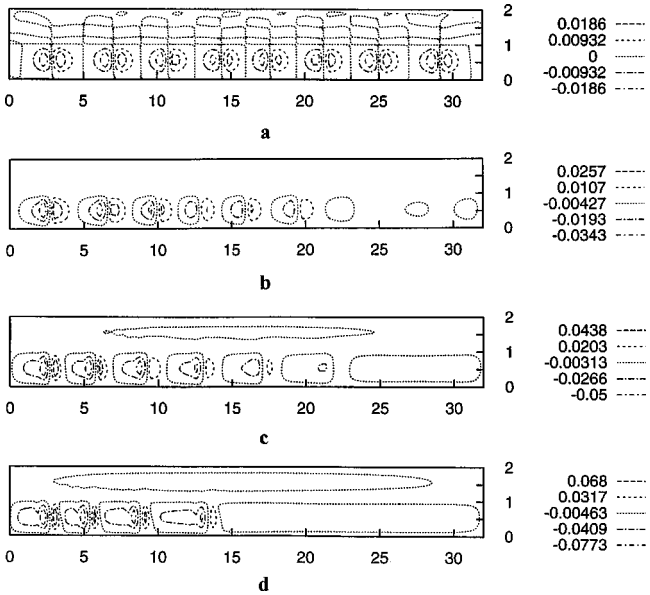

FIG. 13. Streamlines for $\mathrm{Gr}=15\,000$, $\mathrm{Gr}_Q=-15\,000$, $L=32$: (a) $\epsilon=0$, (b) $\epsilon=0.003$, (c) $\epsilon=0.01$, (d) $\epsilon=0.025$.

$$z=0. \tag{A1}$$

The nondimensional boundary condition (13) has the form

$$\eta\phi_1=\phi_2+\frac{\eta \mathrm{M}}{\mathrm{Pr}}\frac{\partial T_1}{\partial x}, \tag{A2}$$

where the Marangoni number

$$\mathrm{M}=\left(-\frac{d\sigma}{dT}\right)\frac{\theta_{a_1}}{\nu_1\chi_1}. \tag{A3}$$

In order to estimate the influence of the thermocapillary effect on the convective flows, let us consider the parallel flow in the system of infinite layers ($L\to\infty$). Solving the system of equations and boundary conditions (8)–(15), (A2) under the assumptions

$$\psi_m=\psi_m(z), \quad T_m=-\epsilon x+T_m^{(0)}(z)+\theta_m(z), \tag{A4}$$

where $T_m^{(0)}(z)$ are given by Eqs. (16) and (17), we find

$$\psi_1(z)=-\frac{\mathrm{Gr}}{24}\left[z^4-z^3\frac{4\beta+3\beta\eta a+\nu a^3}{2\beta(1+\eta a)}+z^2\frac{\beta+\nu a^3}{\beta(1+\eta a)}+z\frac{(\beta\eta-\nu a^2)a}{2\beta(1+\eta a)}\right]-\frac{\mathrm{M}\epsilon\eta a}{4(1+\eta a)\mathrm{Pr}}(z^3-2z^2+z), \tag{A5}$$

$$\psi_2(z)=-\frac{\mathrm{Gr}}{24\beta}\left[\nu z^4+z^3\frac{3a^2\nu+4a^3+\beta\eta}{2a(1+\eta a)}+z^2\frac{(\nu a^3+\beta)\eta}{1+\eta a}+z\frac{(\beta\eta-\nu a^2)a}{2(1+\eta a)}\right]-\frac{\mathrm{M}\epsilon\eta}{4a(1+\eta a)\mathrm{Pr}}(z^3+2az^2+a^2z), \tag{A6}$$

$$\begin{aligned}\theta_1(z)=\mathrm{Pr}(z-1)\Bigg\{&\frac{\mathrm{Gr}^2}{24}\left[\frac{z^4}{5}-z^3\frac{12\beta+7\beta\eta a+5\nu^3 a}{40\beta(1+\eta a)}+z^2\frac{4\beta+25\nu a^3-21\beta\eta a}{120\beta(1+\eta a)}+z\frac{4\beta-5\nu a^3+9\beta\eta a}{120\beta(1+\eta a)}\right.\\&\left.+a\frac{\kappa(4\beta-5\nu a^3+9\beta\eta a)-\chi a^2(4\nu a^3-5\beta\eta+9\nu a^2)}{120\beta(1+\eta a)(1+\kappa a)}\right]+\frac{\mathrm{M}\epsilon^2\eta a}{4\mathrm{P}(1+\eta a)}\left[\frac{z^3}{4}-\frac{5z^2}{12}+\frac{z}{12}+\frac{a(\kappa+\chi a)}{12(1+a\kappa)}\right]\Bigg\},\end{aligned} \tag{A7}$$

$$\begin{aligned}\theta_2(z)=\mathrm{Pr}(z+a)\Bigg\{&\frac{\mathrm{Gr}\epsilon^2\chi}{24\beta}\left[\frac{\nu z^4}{5}+\frac{7\nu a^2+12a^3\nu\eta+5\beta\eta}{40a(1+\eta a)}z^3+\frac{4\nu\eta a^3+25\beta\eta-21\nu a^2}{120(1+\eta a)}z^2+\frac{a(5\beta\eta-9\nu a^2-4\nu\eta a^3)}{120(1+\eta a)}z\right.\\&\left.-\frac{\kappa(4\beta-5\nu a^3+9\beta\eta a)-\chi a^2(9\nu a^2+4\nu\eta a^3-5\beta\eta)}{120\chi(1+\eta a)(1+\kappa a)}\right]+\frac{\mathrm{M}\epsilon^2\eta\chi}{4a(1+\eta a)}\left[\frac{z^3}{4}+\frac{5az^2}{12}+\frac{a^2z}{12}-\frac{a^2(\kappa+\chi a)}{12\chi(1+\kappa a)}\right]\Bigg\}.\end{aligned} \tag{A8}$$

One can see that the expressions for $\psi_m(z)$, $\theta_m(z)$ consist of two parts: the part proportional to Gr which describes the contribution of the buoyancy convection, and the part proportional to M/Pr, which describes the contribution of the thermocapillary convection. The latter can be neglected if

$$\frac{\mathrm{M}}{\mathrm{GrPr}}=\frac{(-d\sigma/dT)}{g\beta_1 a_1^2}\ll 1.$$

That means that the thermocapillary effect can be neglected in comparison to the buoyancy effect, if the thicknesses of the layers are sufficiently large.

[1] G. Z. Gershuni and E. M. Zhukhovitsky, *Convective Stability of Incompressible Fluid* (Nauka, Moscow, 1972).

[2] P. Welander, Tellus **16**, 349 (1964).

[3] G. Z. Gershuni and E. M. Zhukhovitsky, Fluid Dyn. **15**, 816 (1980).

[4] I. B. Simanovskii, Ph.D. thesis, Leningrad State University, 1980.

[5] G. Z. Gershuni, E. M. Zhukhovitsky, and I. B. Simanovskii, *Convective Flows* (Perm Pedagogical Institute, Perm, Russia, 1981), pp. 3–11.

[6] I. B. Simanovskii, D.Sc. thesis, Moscow Physical-Technical Institute, 1991.

[7] A. A. Nepomnyashchy and I. B. Simanovskii, Izv. Akad. Nauk SSSR, Mekh. Zhidk. Gaza **3**, 16 (1990).

[8] O. V. Perestenko and L. Kh. Ingel, Izv., Acad. Sci., USSR, Atmos. Oceanic Phys. **27**, 408 (1991).

[9] O. V. Perestenko and L. Kh. Ingel, J. Fluid Mech. **287**, 1 (1995).

[10] A. A. Nepomnyashchy, I. B. Simanovskii, and L. M. Braverman, Phys. Fluids **12**, 1129 (2000).

[11] A. A. Nepomnyashchy and I. B. Simanovskii, Eur. J. Mech. B/Fluids **20**, 75 (2001).

[12] I. B. Simanovskii and A. A. Nepomnyashchy, *Convective In-*

stabilities in Systems with Interface (Gordon and Breach, London, 1993).
[13] J. E. Weber, Int. J. Heat Mass Transf. **16**, 961 (1973).
[14] J. E. Weber, J. Fluid Mech. **87**, 65 (1978).
[15] R. E. Kelly, Adv. Appl. Mech. **31**, 35 (1994).
[16] S. H. Davis, Annu. Rev. Fluid Mech. **19**, 403 (1987).
[17] A. A. Nepomnyashchy, I. B. Simanovskii, and L. M. Braverman, J. Fluid Mech. **442**, 141 (2001).
[18] T. V. Kuskova and L. A. Chudov, Comput. Methods Program. **11**, 27 (1968).
[19] J. Burguete, N. Mukolobwiez, F. Daviaud, N. Garnier, and A. Chiffaudel, Phys. Fluids **13**, 2773 (2001).
[20] J. Priede and G. Gerbeth, Phys. Rev. E **56**, 4187 (1997).
[21] P. G. Drazin and W. H. Reid, *Hydrodynamic Stability* (Cambridge University Press, Cambridge, 1981).
[22] M. G. Velarde, A. A. Nepomnyashchy, and M. Hennenberg, Adv. Appl. Mech. **37**, 168 (2001).